Second-Harmonic Generation of Single $BaTiO_3$ Nanoparticles down to 22 nm Diameter

Eugene Kim,[†,§] Andrea Steinbrück,[†] Maria Teresa Buscaglia,[‡] Vincenzo Buscaglia,[‡] Thomas Pertsch,[†] and Rachel Grange[†,*]

[†]Institute of Applied Physics, Abbe Center of Photonics, Friedrich Schiller University Jena, Max-Wien-Platz 1, 07743 Jena, Germany and [‡]Institute for Energetics and Interphases, Department of Genoa, National Research Council, Via de Marini 6, I-16149 Genoa, Italy. [§]Present address: Vollmer Lab of Nanophotonics and Biosensing, Max-Planck Institute for Science of Light, Günther-Scharowsky-Str. 1, 91058 Erlangen, Germany.

ABSTRACT We investigate the second-harmonic generation (SHG) signal from single $BaTiO_3$ nanoparticles of diameters varying from 70 nm down to 22 nm with a far-field optical microscope coupled to an infrared femtosecond laser. An atomic force microscope is first used to localize the individual particles and to accurately determine their sizes. Power and polarization-dependent measurements on the individual nanoparticles reveal a diameter range between 30 and 20 nm, where deviations from bulk nonlinear optical properties occur. For 22 nm diameter particles, the tetragonal crystal structure is not applicable anymore and competing effects due to the surface to volume ratio or crystallographic modifications are taking place. The demonstration of SHG from such small nanoparticles opens up the possibilities of using them as bright coherent biomarkers. Moreover, our work shows that measuring the SHG of individual nanoparticles reveals critical material properties, opening up new possibilities to investigate ferroelectricity at the nanoscale.

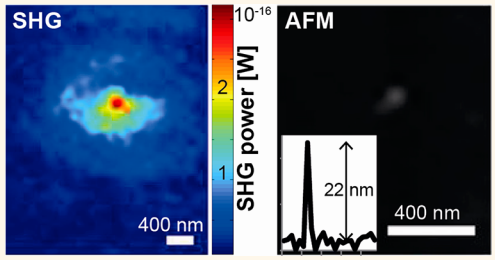

KEYWORDS: nanoparticle · barium titanate · second-harmonic generation · ferroelectricity · biomarker

Understanding the properties of materials at the nanoscale is important for developing powerful applications in life sciences or optoelectronics. At such small sizes, deviations from bulk properties can be expected since the material is strongly confined and surface instead of volume effects tend to dominate. Moreover, crystallographic transitions may occur, with important consequences on certain materials that may lose their particular characteristics. Such materials are, for instance, noncentrosymmetric crystals like barium titanate ($BaTiO_3$), widely used in the electronic industry[1] and more recently exploited in bioimaging for their strong second-order nonlinear optical property as bulk and down to 100 nm in diameter.[2,3] Modifications of the ferroelectricity and crystallography with sizes have been under investigation for many years,[4−7] giving sometimes not unique results due to properties highly dependent on the synthesis method. The size at which those properties may change is then critical to ensure the success of their future applications as high density memories or biomarkers.

Most of the aforementioned studies are focused on the electronic and structural characteristics of $BaTiO_3$ using X-ray diffraction,[4,8] conductance measurements,[5] Raman spectroscopy,[6] or high-resolution techniques as electron holography.[7] To our knowledge, no investigations of the nonlinear optical properties have been performed on $BaTiO_3$ particles below 50 nm in diameter.

Here, we study the second-harmonic generation (SHG) signal from single $BaTiO_3$ nanoparticles with diameters varying from 70 down to 22 nm using a far-field optical microscope. Exploiting power and polarization-dependent responses of single nanoparticles with different sizes, we will discuss the deviations from nonlinear optical bulk properties. Even if our measurements are limited to a few nanoparticles, we show that nonlinear optical SHG measurement can become a useful tool in the material science community since it brings new insights

* Address correspondence to rachel.grange@uni-jena.de.

Received for review March 8, 2013 and accepted May 21, 2013.

Published online May 21, 2013
10.1021/nn401198g

in the investigation of the crystallography at the nanoscale.

Our investigation can significantly impact the use of the so-called harmonic nanoprobes as contrast agents for nonlinear bioimaging applications.[9] Indeed, besides the well-known fluorescence mechanism in dyes or protein, harmonic generation is a nonlinear optical effect with great potential for sustainable, tunable, coherent,[2,10] and biocompatible imaging.[11] However, up to now, the size of the harmonic nanoprobes (usually ranging from 70 to 100 nm in diameters)[11] may have prevented their use among the life science community. Moreover, several studies have revealed the biocompatibility of $BaTiO_3$,[11,12] which may open up a bright future for this material as coherent biomarkers in parallel to the electronic industry.

Particle Synthesis and Colloidal Suspension. Ultrafine $BaTiO_3$ nanoparticles were prepared by solution precipitation.[13,14] These nanoparticles were first used as precursors for the preparation of dense nanoceramics.[15] The X-ray diffraction (XRD) suggests that the powder is pseudocubic, but the exact symmetry is difficult to determine because of the broadening of the diffraction peaks due to the small particle size (Figure S1 in Supporting Information).[4] Indeed, by decreasing the grain size, we showed that the tetragonality is reduced, too. However, since an anomalous broadening of the XRD peaks remains, the material is not cubic.

The specific surface area of the powder is 75 $m^2 g^{-1}$, corresponding to a mean particle size of 16 nm. The transmission electron microscope (TEM) image (inset of Figure 1) confirms particles with diameters well below 50 nm. Observation at high resolution (Figure S2 in Supporting Information) shows that the particles correspond to single nanocrystals. Starting from a dried powder, we first functionalized the surface of the $BaTiO_3$ nanoparticles with primary amine using aminopropyltriethoxysilane (APTES) to obtain a stable colloidal suspension in an ethanol/water solution (2/1) as previously demonstrated.[3] We then performed size distribution measurement with dynamic light scattering (DLS) method, giving a peak centered at 32 nm (Figure 1). This result indicates that the particles are weakly agglomerated and that the functionalization is successful. Indeed, the nanoparticles did not precipitate even after a few days of suspension. Agglomeration is also responsible for the tail of the size distribution.

Optical Transmission Microscope. For the detection and characterization of the SHG signal from single $BaTiO_3$ nanoparticles, a transmission optical microscope was built by modifying a commercial upright microscope (Zeiss Axio Imager M2m). Figure 2 depicts the configuration of the setup. A Ti:sapphire femtosecond pulsed laser (80 MHz repetition rate and about 300 fs pulse duration at the sample position) was used as an excitation beam. The reason for using such a high

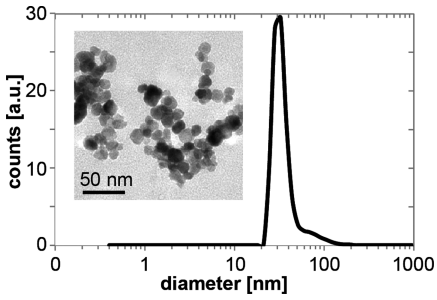

Figure 1. Size distribution of ultrafine $BaTiO_3$ powder based on DLS measurements. The inset shows a typical TEM image of the nanoparticles.

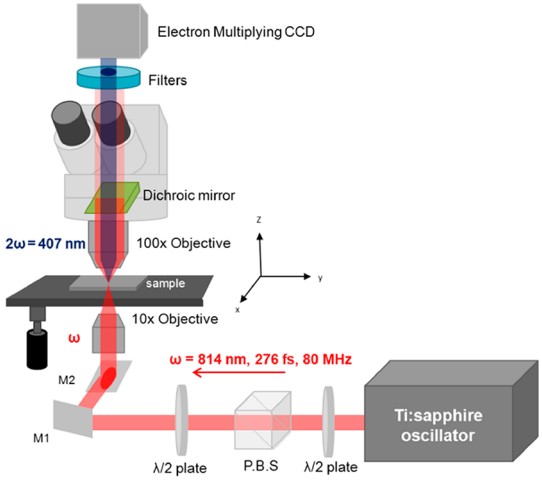

Figure 2. Modified upright transmission microscope for SHG measurements with a wide excitation area (see detailed description in the text).

intensity laser arises from the originality of the SHG mechanism, which requires the simultaneous absorption of two photons without involving any real energy state. The laser wavelength is set as 814 nm to match the band-pass filter centered at 407 nm with a bandwidth of 17 nm. The incident beam propagates first through a polarization beam splitter (PBS) which only transmits p-polarized light. Then it goes through a half-wave plate that allows varying the angle of the polarization. Afterward, the beam is focused to 3.2 μm in diameter by an objective (10×, numerical aperture (NA) = 0.2) onto the sample plane, and the emission of SHG occurs. The emitted SHG light and the incident light are then collected by a 100× oil immersion objective (Nikon E-Plan 100× oil, NA 1.25). The path of both beams is separated by a dichroic mirror placed right after the objective. It transmits the emitted light and reflects most of the incident light. After passing through the dichroic mirror, the small amount of the incident beam, which was still transmitted, is filtered out by a short-pass filter (BG39) and the band-pass filter. The SHG signal is recorded with an electron multiplying charge-coupled device (EMCCD, Andor iXonEM+2885). A motorized stage (Zeiss, motorized stage *XY* step CAN) with step sizes of 200 nm was used

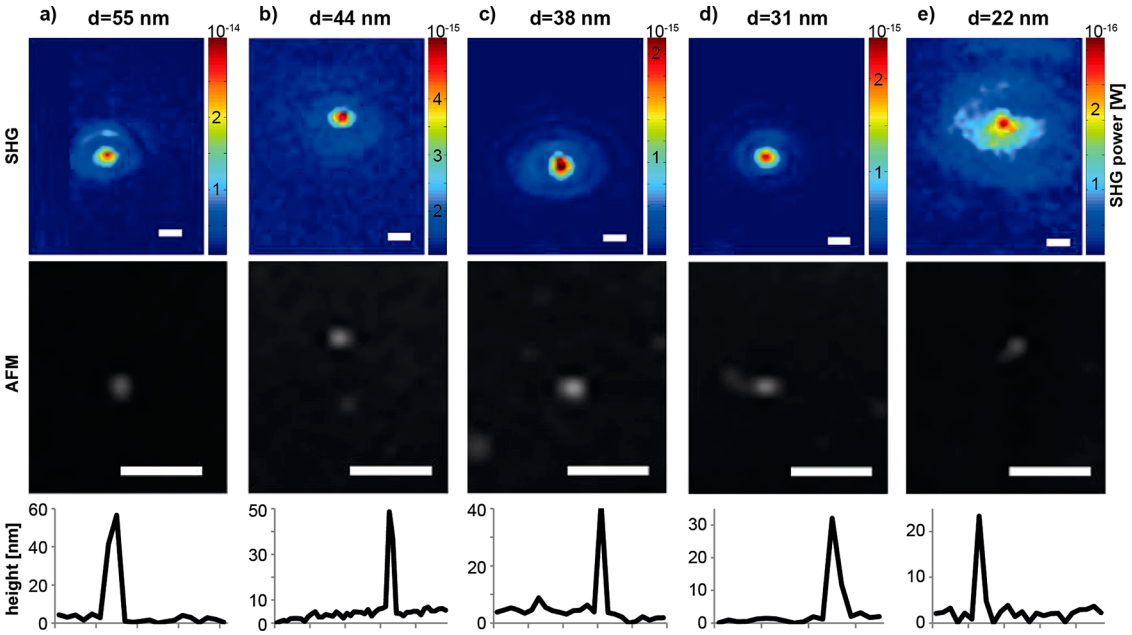

Figure 3. Measured SHG responses (top row) and corresponding AFM images (middle row) of five isolated $BaTiO_3$ nanoparticles with diameters of (a) 55, (b) 44, (c) 38, (d) 31, and (e) 22 nm, determined with the height profile extracted from the AFM images (bottom row). The scale bars are 400 nm.

for the control of the horizontal position, and the motorized drive of the upright microscope with a step size of 25 nm was used for the vertical axis movement.

The modified transmission setup offers several advantages for single-particle imaging, as we recently showed for individual nanowire measurements.[16] A larger excitation spot allows images to be taken without scanning, which is much faster. Moreover, the transmission setup makes the modeling of the excitation behavior much simpler by avoiding a tightly focused beam regime that adds complex polarization components. In our theoretical model, which is detailed below, the excitation beam is assumed to be a plane wave, meaning that the longitudinal field component of the beam is not considered. However, when the excitation beam is focused by a high NA objective like in a standard upright microscope, the field is no longer a plane wave and it contains the nonvanishing longitudinal component. When the beam experiences this kind of distortion after the high NA objective, it is called a tightly focused regime.[17] This longitudinal component can significantly affect the response of the nanoparticles because of the tensorial nature of SHG. Since we cannot control the orientation of the nanoparticles lying on the substrates, we prefer the wide illumination configuration.

EXPERIMENTAL RESULTS

In Figure 3, we show the SHG responses (top row) of five different $BaTiO_3$ nanoparticles and their corresponding AFM images (middle row), which are used to determine the respective diameters of (a) 55, (b) 44, (c) 38, (d) 31, and (e) 22 nm from the height measurements (bottom row). The AFM images ensure that the SHG signals are from single, well isolated particles within the diffraction limit ($D = \lambda/(2\ \mathrm{NA}) = 162.8$ nm), where $\lambda = 407$ nm. The only exception would be Figure 3d, where another particle is placed about 200 nm away from our target particle. However, this particle is as small as 12 nm in diameter, and therefore, the corresponding SHG signal should be negligible.

The SHG images of Figure 3 are taken by a cooled EMCCD with 2 s of exposure time and the gain factor of 200. Each image is accumulated 10 times and averaged. The cooling temperature of the camera is set to −80 °C for the suppression of thermal noise. The laser polarization is adjusted for each nanoparticle in order to obtain the maximum signal and comparable results. The peak intensity at the sample position was (a) 149, (b) 158.5, (c) 158.1, (d) 159.6, and (e) 228 GW/cm^2 for the respective nanoparticles shown in Figure 3. One can observe that the SHG intensity from the 22 nm $BaTiO_3$ nanoparticle (Figure 3e) is extremely weak and the background SHG from the glass substrate appears.

The amount of SHG power from the $BaTiO_3$ nanoparticles is related to the orientation of the crystal axis of the $BaTiO_3$ as well as their sizes. Since the sizes are much smaller than the excitation wavelength, the nanoparticles are seen as Rayleigh particles with no phase matching conditions. However, the particles are too big to be considered as point sources as in an incoherent Rayleigh regime (usually objects below 5−10 nm). Therefore, we are not in the presence of hyper-Rayleigh scattering (HRS) but coherent SHG.[18] As detailed in our previous model used for 100 nm

$BaTiO_3$ nanoparticles,[2] and assuming spherical particles,[19] the total emitted power is proportional to the square of the particle volume. Thus, for decreasing sizes, the SHG intensity decreases with the power of 6 of the particle radius. In Figure 4, we display the amount of SHG power of each $BaTiO_3$ nanoparticles as measured in Figure 3 *versus* their sizes. The data are following a power of 6 fit as expected from the model. Note that a higher order fit may match those results, too, but the trend is clearly showing a drop in SHG power according to a 6th power. We do not observe a strong deviation for the smallest particles, where the surface effects may play a stronger role. Even though the influence of the SHG from the glass substrate is negligible for particles above 30 nm, it starts to play an important role for the smallest nanoparticle, as shown from the error bars of Figure 4. Furthermore, we are close to reaching the lowest sensitivity of the EMCCD camera.

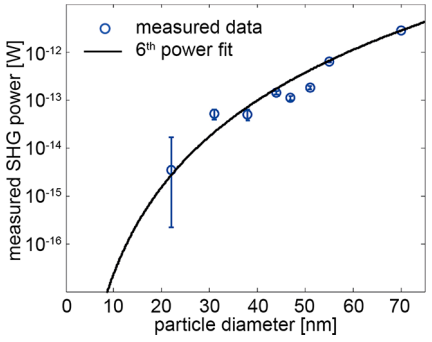

Figure 4. Relation of $BaTiO_3$ nanoparticle diameters and the logarithm of the SHG power. The blue dots represent the measured power from particles of Figure 3 and three additional measurements with their corresponding fit of the 6th power (solid line). The error bars show the SHG contribution from the glass substrate.

In order to ensure that the detected signal is indeed from the SHG process, power dependency measurements were conducted at average incident power of 50 to 700 mW for each of the five studied nanoparticles (Figure 5). Particles with diameters from 55 down to 38 nm show a typical quadratic behavior, indicating that the signal is generated from a second-order nonlinear process (Figure 5a–c). Particles with 31 and 22 nm diameters (Figure 5d,e) are also well fitted with a quadratic curve; however, the data are not as curved as the bigger particles and may well follow an almost linear behavior. It is particularly obvious for the 22 nm one. This result is a first indication that some effect other than volume SHG is taking place for particle diameters around 30 nm and smaller. However, due to the smooth transition that we observed, several processes might be competing at sizes below 30 nm. Above this size, no discrepancies are seen with an expected quadratic process. To complete the analysis, we added a table in Figure 5 with the coefficient of determination R^2 for quadratic and linear fitting of the experimental data. For the quadratic fit, the best R^2 (closest to 1) is obtained for the biggest particle and decreases with the particle size (first column of the table in Figure 5). On the contrary, for the linear fit, the best R^2 is obtained for the smallest particle and then decreases with increasing particle sizes (second column of the table in Figure 5). We also like to mention that the experimental data of Figure 5 show no saturation behavior even at the highest excitation power. Therefore, we are confident that thermal heating is not affecting the nanocrystals.

Then, we performed polarization-dependent measurements on each of the particles in order to see any deviation from the expected tensor response of bulk $BaTiO_3$, which has a tetragonal structure at room

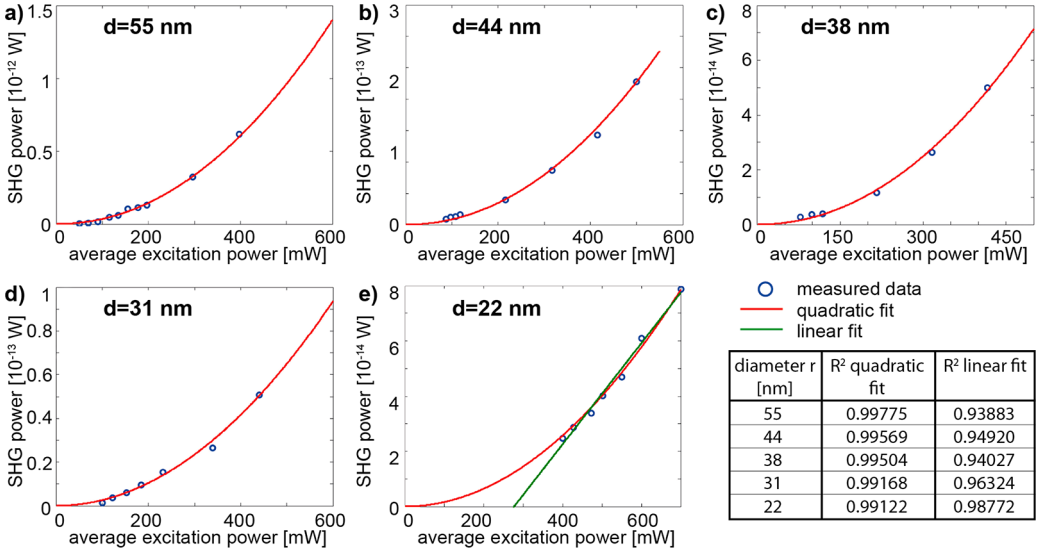

diameter r [nm]	R^2 quadratic fit	R^2 linear fit
55	0.99775	0.93883
44	0.99569	0.94920
38	0.99504	0.94027
31	0.99168	0.96324
22	0.99122	0.98772

Figure 5. SHG power dependency for the five isolated $BaTiO_3$ nanoparticles with diameters of (a) 55, (b) 44, (c) 38, (d) 31, and (e) 22 nm. Table with corresponding coefficient of determination R^2 for quadratic and linear fits.

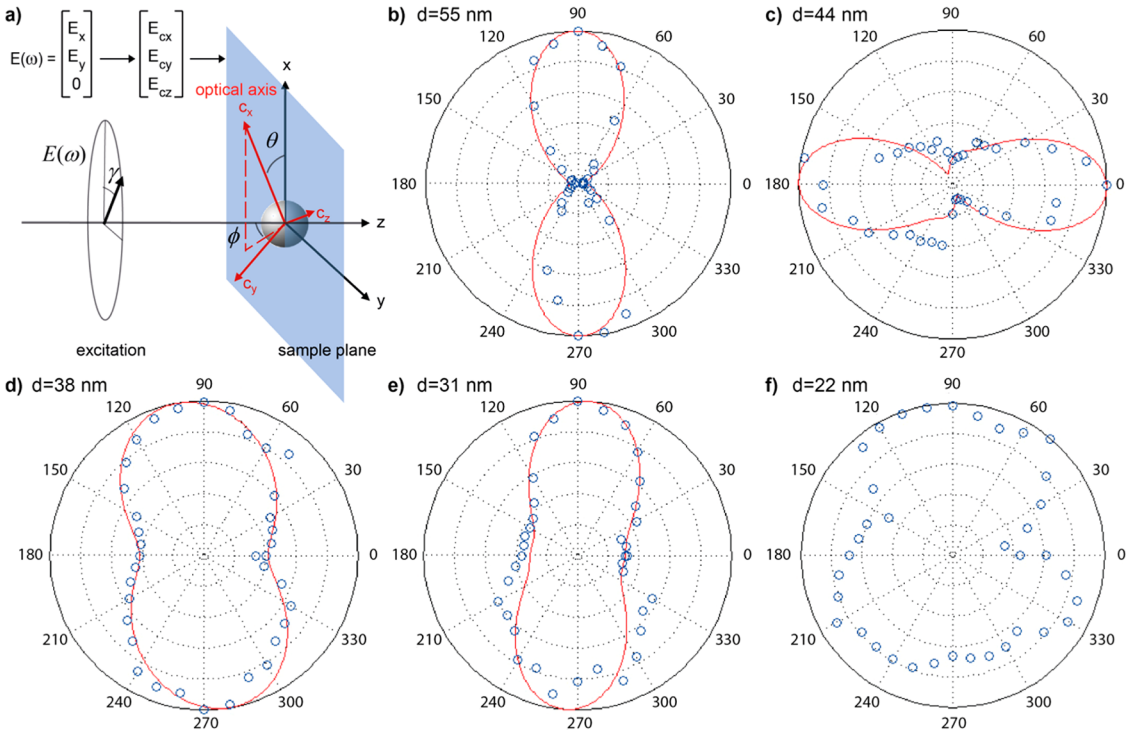

Figure 6. (a) Scheme of the $BaTiO_3$ nanocrystal reference frame and the incident light used for the calculation of SHG polarization response (red curves) fitting the measurements (blue dots) of single $BaTiO_3$ nanoparticles of diameters (b) 55, (c) 44, (d) 38, (e) 31, and (f) 22 nm. All units are in degrees.

temperature and a single optical axis, the so-called *c*-axis.[20] Like any other uniaxial crystal, $BaTiO_3$ has a rotational symmetry respective to the *c*-axis. A change of the orientation between the polarization of the incident light and the *c*-axis of the $BaTiO_3$ crystal generates a different amount of SHG signal. In other words, the SHG response will be determined only by the orientation of the *c*-axis, which can be related to the laboratory frame (*x*,*y*,*z*) by the angles θ and ϕ, as depicted in Figure 6a. The incident light is assumed to be a plane wave, which propagates along the *z*-axis having electric field components E_x and E_y. This incident field defined in normal Cartesian coordinates has to be first projected onto the crystal coordinate system (c_x,c_y,c_z). After the conversion of the coordinate system, the SHG polarization can be calculated by simply using the second-order polarization $\vec{P}(2\omega) = \varepsilon_0\chi^{(2)}\vec{E}(\omega)^2$, where ε_0 is the permittivity of the free space, $\chi^{(2)}$ the second-order susceptibility tensor composed of 18 d_{il} coefficients ($i = 1-3$ and $l = 1-6$), E the incident field, and ω the frequency of the incident light. In the simulation, the SHG signal was calculated by using the following tensor coefficients of bulk $BaTiO_3$: d_{15} = 17 pm/V, d_{31} = 15.7 pm/V, and d_{33} = 6.8 pm/V.[21]

The measurement of the polarization-dependent SHG response was conducted for each $BaTiO_3$ nanoparticle of Figure 3. We changed the angle of the incident polarization by rotating a half-wave plate by steps of 5° and captured the SHG images for each position. Figure 6b–f shows the results of polarization-dependent measurements together with the calculated fitting based on the bulk tensor parameters. It was possible to fit the particles from 55 down to 31 nm with some slight discrepancies, showing that $BaTiO_3$ nanoparticles still keep their tetragonal bulk crystallography (Figure 6b–e). Moreover, the simulation also reveals the information on the orientation of the *c*-axis of each particle defined by θ and ϕ, which are $\theta = 46.4°$ and $\phi = 37.7°$ for 55 nm, $\theta = 115.2°$ and $\phi = 137.5°$ for 44 nm, $\theta = 35°$ and $\phi = 164°$ for 38 nm, and $\theta = 46.4°$ and $\phi = 68.8°$ for 31 nm $BaTiO_3$ nanoparticles. Here, it should be noted that there are $\pm 180°$ of ambiguity because of the symmetry of the material. Nevertheless, it was not possible to obtain a matching fit for the 22 nm $BaTiO_3$ nanoparticles (Figure 6f). This is probably highly related to the change of the crystallography of $BaTiO_3$ and the corresponding effect on the SHG signal at such a small size. Furthermore, we cannot exclude that the shape of the particle plays a role in the quality of the fitting. Since our model assumes spherical shapes, some discrepancy may occur in the fitting due to different nanoparticle shapes.

DISCUSSION

$BaTiO_3$ nanoparticles above 100 nm are commonly accepted as they have bulk-like properties. That is, their crystallography at room temperature is tetragonal, and the transition from ferroelectric tetragonal to paraelectric cubic phase occurs at 120 °C (Curie temperature, T_c), which is the same as the bulk

$BaTiO_3$ Curie temperature. Meanwhile, the phase transition of $BaTiO_3$ nanoparticles below 100 nm has not been well-established yet, and a thorough debate is still in progress. The concentration and nature of lattice defects in the perovskite lattice as well as the presence of extended defects (grain boundaries, pores) is strongly dependent on the synthesis method (temperature, solvent, counterions, *etc.*), and this explain the broad dispersion of experimental data. Some researchers report that the Curie temperature drops with decreasing grain size of $BaTiO_3$; therefore, there exists a size limit where the $BaTiO_3$ loses its ferroelectricity at room temperature.[22−24] In contrast, some argue that the size limit does not exist but rather the ferroelectricity weakens exponentially with size.[25] Others suggest that $BaTiO_3$ nanoparticles are composed of a tetragonal core region and a cubic shell region where the tetragonal phase is relaxed to be energetically stable, and they claim that when the size decreases the surface dominates over the volume; that is, the cubic shell region dominates the tetragonal core region.[6,8] In any case, the existence of a disordered nonpolar surface layer is generally accepted. We are aware that the nonlinear optical measurement of few single particles is not enough to draw straight conclusions, but on the basis of the clear discrepancy of our results for the 22 nm, we can contribute to the debate about the possible crystalline form of nanoscale $BaTiO_3$. If we apply the respective arguments described above to our experimental results, we can think of three different scenarios for the theoretical modeling of $BaTiO_3$ nanoparticles below 31 nm. The first scenario is to regard the $BaTiO_3$ nanoparticle as a pure cubic structure. This means that we need to take into account the multipolar contribution from the volume and the surface contribution for the SHG modeling. The second scenario would be to keep the modeling based on tetragonal structure but to consider the surface SHG in addition. The last one is to apply the core−shell structure into our modeling. In this case, the dipolar contribution from the volume of the tetragonal core, the multipolar contribution from the volume of the cubic shell, and the extrinsic surface SHG should be considered.

As recently reported,[6] the volume effect dominates over the surface for a diameter of 220 ± 140 nm; there is a competition between the volume and the surface for 47 ± 11 nm and the dominance of the surface over the volume for 16 ± 4 nm of $BaTiO_3$ nanoparticles. Our data indicate that, at the size of 38 nm, the volume effect still dominates. There is some competition at 31 nm (Figure 5d), and no bulk fit is possible at all for 22 nm nanoparticles (Figure 6f). Therefore, the transition between the crystallographic structures or the volume *versus* surface effects occurs in our case between 31 and 22 nm. Considering that the synthesis methods of the $BaTiO_3$ nanocrystals are totally different, their method being based on a molten salt synthesis[6] and our procedure on an hydrothermal-like chemical synthesis,[4] the results tend to the same range of sizes with only a slight discrepancy. Anyhow, if we assume that the cubic surface dominates over the tetragonal volume at around 20 nm size, as suggested in ref 6, it is worth trying the theoretical modeling based on our first scenario, a pure cubic structure, particularly for the 22 nm $BaTiO_3$ nanoparticle. However, the hyperpolarizability tensor for the cubic $BaTiO_3$ nanoparticles needs to be defined in advance,[26] which is planned for a future work.

CONCLUSION

We demonstrate SHG from individual $BaTiO_3$ nanoparticles with diameters spanning from 70 down to 22 nm. The SHG signal decreases with the 6th power of the particle sizes, which is in agreement with our model considering volume effects. Moreover, each particle shows a quadratic dependency of the SHG with the incident beam power; however, for 31 and 22 nm, the curvature of the results is not so clear, showing some additional competing effects. By measuring the polarization response of the SHG signal for each nanoparticle, we can conclude that between 31 and 22 nm diameters a change occurs since the bulk parameters of tetragonal $BaTiO_3$ do not match the smallest particle response at all. We proposed several interpretations of the change, which still need further investigations. Nevertheless, we are convinced that, starting from 30 nm, surface effects as well as a nontetragonal crystal structure play an increasing role, which tends to dominate around 20 nm.

METHODS

Sample Preparation. After dilution and ultrasonification of the colloidal suspension, we deposited 5 μL of the functionalized $BaTiO_3$ onto a precleaned silica glass substrate where gold grids with coordinates were patterned on the surface by electron-beam lithography. The patterned substrate was used to retrieve the position of the isolated particles measured first by atomic force microscopy (AFM) to determine their sizes and then in the nonlinear optical microscopy setup. After the solution was dried, we dropped PMMA (polymethyl methacrylate, 2% in (−)-ethyl-L-lactate) solution on the sample using spin coating at 500 rpm. The speed was then increased to 2000 rpm for 1 min to obtain a homogeneous 100 nm thick PMMA layer. Afterward, the PMMA-coated sample was heated for 20 min at 80 °C to cross-link the polymer. The additional PMMA layer was used to match the refractive index with the oil immersion and to have the best collection efficiency. Finally, the sample was covered by a coverslip and sealed as protection from the immersion oil used during the optical measurement.

Conflict of Interest: The authors declare no competing financial interest.

Acknowledgment. This work was financially supported by the German Federal Ministry of Education and Research *via* the project PhoNa and the Thuringian State Government *via* the project MeMa, as well as by the Carl Zeiss foundation. The authors give thanks to the Leibniz Institute of Age Research—Fritz Lipmann Institute in Jena, Germany, for providing access to the TEM, Katrin Buder for help with TEM measurements, as well as the Institute of Photonic Technology for allowing the use of the zeta sizer. We thank Anton Sergeyev for the preparation of the figures.

Supporting Information Available: XRD graph and high-resolution TEM image for $BaTiO_3$ nanoparticles. This material is available free of charge *via* the Internet at http://pubs.acs.org.

REFERENCES AND NOTES

1. Scott, J. F. Applications of Modern Ferroelectrics. *Science* **2007**, *315*, 954–959.
2. Hsieh, C.-L.; Grange, R.; Pu, Y.; Psaltis, D. Three-Dimensional Harmonic Holographic Microcopy Using Nanoparticles as Probes for Cell Imaging. *Opt. Express* **2009**, *17*, 2880–2891.
3. Pu, Y.; Grange, R.; Hsieh, C.-L.; Psaltis, D. Nonlinear Optical Properties of Core—Shell Nanocavities for Enhanced Second-Harmonic Generation. *Phys. Rev. Lett.* **2010**, *104*, 207401–207405.
4. Buscaglia, V.; Buscaglia, M. T.; Viviani, M.; Mitoseriu, L.; Nanni, P.; Trefiletti, V.; Piaggio, P.; Gregora, I.; Ostapchuk, T.; Pokorny, J.; *et al.* Grain Size and Grain Boundary-Related Effects on the Properties of Nanocrystalline Barium Titanate Ceramics. *J. Eur. Ceram. Soc.* **2006**, *26*, 2889–2898.
5. Lomax, J. F.; Fontanella, J. J.; Edmondson, C. A.; Wintersgill, M. C.; Westgate, M. A.; Eker, S. Size Effects Observed *via* the Electrical Response of $BaTiO_3$ Nanoparticles in a Cavity. *J. Phys. Chem. C* **2012**, *116*, 23742–23748.
6. Szwarcman, D.; Vestler, D.; Markovich, G. The Size-Dependent Ferroelectric Phase Transition in $BaTiO_3$ Nanocrystals Probed by Surface Plasmons. *ACS Nano* **2011**, *5*, 507–515.
7. Polking, M. J.; Han, M.-G.; Yourdkhani, A.; Petkov, V.; Kisielowski, C. F.; Volkov, V. V; Zhu, Y.; Caruntu, G.; Alivisatos, A. P.; Ramesh, R. Ferroelectric Order in Individual Nanometre-Scale Crystals. *Nat. Mater.* **2012**, *11*, 700–709.
8. Hoshina, T.; Wada, S. Composite Structure and Size Effect of Barium Titanate Nanoparticles. *Appl. Phys. Lett.* **2008**, *93*, 192914.
9. Bonacina, L. Nonlinear Nanomedecine: Harmonic Nanoparticles toward Targeted Diagnosis and Therapy. *Mol. Pharmaceutics* **2013**, *10*, 783–792.
10. Hsieh, C.-L.; Pu, Y.; Grange, R.; Laporte, G.; Psaltis, D. Imaging through Turbid Layers by Scanning the Phase Conjugated Second Harmonic Radiation from a Nanoparticle. *Opt. Express* **2010**, *18*, 20723–20731.
11. Staedler, D.; Magouroux, T.; Hadji, R.; Joulaud, C.; Extermann, J.; Schwung, S.; Passemard, S.; Kasparian, C.; Clarke, G.; Gerrmann, M.; *et al.* Harmonic Nanocrystals for Bio-labeling: A Survey of Optical Properties and Biocompatibility. *ACS Nano* **2012**, *6*, 2542–2549.
12. Ciofani, G.; Danti, S.; D'Alessandro, D.; Moscato, S.; Petrini, M.; Menciassi, A. Barium Titanate Nanoparticles: Highly Cytocompatible Dispersions in Glycol-Chitosan and Doxorubicin Complexes for Cancer Therapy. *Nanoscale Res. Lett.* **2010**, *5*, 1093–1101.
13. Testino, A.; Buscaglia, M. T.; Buscaglia, V.; Viviani, M.; Bottino, C.; Nanni, P. Kinetics and Mechanism of Aqueous Chemical Synthesis of $BaTiO_3$ Particles. *Chem. Mater.* **2004**, *16*, 1536–1543.
14. Testino, A.; Buscaglia, M. T.; Viviani, M.; Buscaglia, V.; Nanni, P. Synthesis of $BaTiO_3$ Particles with Tailored Size by Precipitation from Aqueous Solutions. *J. Am. Ceram. Soc.* **2004**, *87*, 79–83.
15. Buscaglia, M.; Viviani, M.; Buscaglia, V.; Mitoseriu, L.; Testino, A.; Nanni, P.; Zhao, Z.; Nygren, M.; Harnagea, C.; Piazza, D.; *et al.* High Dielectric Constant and Frozen Macroscopic Polarization in Dense Nanocrystalline $BaTiO_3$ Ceramics. *Phys. Rev. B* **2006**, *73*, 064114.
16. Grange, R.; Brönstrup, G.; Kiometzis, M.; Sergeyev, A.; Richter, J.; Leiterer, C.; Fritzsche, W.; Gutsche, C.; Lysov, A.; Prost, W.; *et al.* Far-Field Imaging for Direct Visualization of Light Interferences in GaAs Nanowires. *Nano Lett.* **2012**, *12*, 5412–5417.
17. Novotny, L.; Hecht, B. *Principles of Nano-Optics*; Cambridge University Press: Cambridge, U.K., 2006.
18. Roke, S.; Gonella, G. Nonlinear Light Scattering and Spectroscopy of Particles and Droplets in Liquids. *Annu. Rev. Phys. Chem.* **2012**, *63*, 353–378.
19. Malmqvist, L.; Hertz, H. M. 2nd-Harmonic Generation in Optically Trapped Nonlinear Particles with Pulsed Lasers. *Appl. Opt.* **1995**, *34*, 3392–3397.
20. Devonshire, A. XCVI. Theory of Barium Titanate. *Philos. Mag.* **1949**, *40*, 1040–1063.
21. Boyd, R. W. *Nonlinear Optics*, 3rd ed.; Academic Press: Burlington, MA, 2008.
22. Fang, C.; Zhou, D.; Gong, S. Core—Shell Structure and Size Effect in Barium Titanate Nanoparticle. *Phys. B* **2011**, *406*, 1317–1322.
23. Spanier, J. E.; Kolpak, A. M.; Urban, J. J.; Grinberg, I.; Ouyang, L.; Yun, W. S.; Rappe, A. M.; Park, H.; Lian, O. Y. Ferroelectric Phase Transition in Individual Single-Crystalline $BaTiO_3$ Nanowires. *Nano Lett.* **2006**, *6*, 735–739.
24. Böttcher, R.; Klimm, C.; Michel, D.; Semmelhack, H.-C.; Völkel, G.; Gläsel, H.-J.; Hartmann, E. Size Effect in Mn^{2+}-Doped $BaTiO_3$ Nanopowders Observed by Electron Paramagnetic Resonance. *Phys. Rev. B* **2000**, *62*, 2085–2095.
25. Petkov, V.; Buscaglia, V.; Buscaglia, M.; Zhao, Z.; Ren, Y. Structural Coherence and Ferroelectricity Decay in Submicron- and Nano-Sized Perovskites. *Phys. Rev. B* **2008**, *78*, 054107.
26. Russier-Antoinc, I.; Benichou, E.; Bachelier, G.; Jonin, C.; Brevet, P. F. Multipolar Contributions of the Second Harmonic Generation from Silver and Gold Nanoparticles. *J. Phys. Chem. C* **2007**, *111*, 9044–9048.